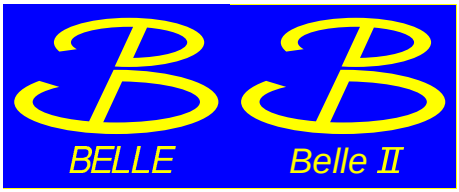

Publication number: BELLE2-PUB-DRAFT-2024-011
Belle II Note: BELLE2-NOTE-PH-2023-049
Authors: L. K. Li, A. J. Schwartz, K. Kinoshita
Referees: M. Staric, M. Nayak, X. B. Ji
PC reader: Y. Sakai
Intended journal: JHEP
KEK preprint: 2024-XX
Belle II preprint: 2024-xxx
Deadline: XX XX, 2024

Search for *CP* violation in $D^+_{(s)} \to K^0_S K^- \pi^+ \pi^+$ decays

Draft version 4.1
July 4, 2024

Abstract

We perform the first search for *CP* violation in $D^+_{(s)} \to K^0_S K^- \pi^+ \pi^+$ decays. We use a combined data set from the Belle and Belle II experiments, which study e^+e^- collisions at a center-of-mass energy on or near the $\Upsilon(4S)$ resonance. The total integrated luminosity is 1407 fb^{-1}. We measure six *CP*-violating asymmetries that are based on triple-products and quadruple products of the momenta of final-state particles, and also the particles' helicity angles. Such asymmetries are sensitive to *CP* violation due to interference among different partial-wave contributions to the decay amplitudes. We obtain a precision of 0.5% for $D^+ \to K^0_S K^- \pi^+ \pi^+$ decays and less than 0.3% for $D^+_s \to K^0_S K^- \pi^+ \pi^+$ decays. No evidence of *CP* violation is found. Our results for the triple-product asymmetries are the most precise to date for singly-Cabibbo-suppressed D^+ decays. Our results for the other asymmetries are the first such measurements performed for charm decays.

1 Introduction

The violation of charge-conjugation plus parity (CP) symmetry holds significant importance in particle physics, as it is essential for explaining the matter-antimatter imbalance in the Universe [1]. Within the Standard Model (SM), the sole source of CP violation (CPV) is a complex phase in the CKM matrix [2]. However, this source is insufficient to explain the observed matter-antimatter imbalance, and thus we conclude there must be other sources of CPV, presumably arising from new physics (NP) beyond the SM.

In the SM, CPV in the charm sector arises at the level of $\mathcal{O}(10^{-3})$ or less [3–5], and observing CPV significantly above this level would be interpreted as a sign of NP [6–9]. Various methods have been used to search for CPV in charm decays [10]: measuring differences in decay widths, searching for differences in decay-time distributions or regions of phase-space, measuring triple-product asymmetries, measuring decay asymmetry parameters in baryonic decays, and performing amplitude analyses and an "energy test" of multi-body decays. To date, the only observation of CPV was reported by LHCb [11], which measured a difference between the asymmetries A_{CP}^{KK} and $A_{CP}^{\pi\pi}$ for $D^0 \to K^+K^-$ and $D^0 \to \pi^+\pi^-$ decays. The observable A_{CP} is the asymmetry between partial widths of a D and a $\overline{D}$; a nonzero value mainly arises from *direct CPV*, i.e., interference between two or more decay amplitudes to the same final state. The effect is proportional to $\sin\delta \sin\phi$, where δ is the strong phase difference between the two amplitudes, and ϕ is the weak phase difference.

Four-body decays of charmed mesons typically proceed via intermediate resonances, and the corresponding amplitudes interfere with one another. Thus, these decays offer a promising opportunity to observe CPV. One observable sensitive to CPV in $D \to h_1\, h_2\, h_3\, h_4$ ($h = \pi, K, \eta$, etc.) decays is the "triple product" $C_{\rm TP} \equiv (\vec{p}_1 \times \vec{p}_2) \cdot \vec{p}_3$, where the momenta $\vec{p}_{1,2,3}$ are measured in the rest frame of the D. The asymmetry ($\mathcal{A}_{CP}^{C_{\rm TP}}$) between $C_{\rm TP}$ and its counterpart $\overline{C}_{\rm TP}$ for the charge-conjugate $\overline{D}$ decay is CP-violating. However, unlike A_{CP}, $\mathcal{A}_{CP}^{C_{\rm TP}}$ is proportional to $\sin\phi\cos\delta$ [12–15], i.e., it reaches its maximum value at $\delta = 0$. Several experiments have searched for CPV using triple-product asymmetries in four-body D decays [10], thus far without success. Here we measure the triple-product asymmetry for the four-body decays $D^+ \to K_S^0 K^- \pi^+ \pi^+$ and $D_s^+ \to K_S^0 K^- \pi^+ \pi^+$. [1] The first mode is singly Cabibbo-suppressed, like the $D^0 \to K^+K^-$, $\pi^+\pi^-$ decays for which CPV was observed. The dominant intermediate process, $D^+ \to \overline{K}^{*0} K^{*+}$, involves tree, annihilation, and "penguin" amplitudes as shown in figure 1. These amplitudes interfere with one another, potentially giving rise to CPV. In addition to measuring the triple-product asymmetry, we also measure the asymmetry for the "quadruple product" $C_{\rm QP} \equiv (\vec{p}_1 \times \vec{p}_2) \cdot (\vec{p}_3 \times \vec{p}_4)$. Quadruple product asymmetries are discussed as a method for measuring CPV in refs. [14–17]. Finally, we measure asymmetries in helicity angle distributions, which can also exhibit CP violation [16, 18]. To date, quadruple-product asymmetries and asymmetries in helicity angle distributions have not yet been studied for multibody charm decays.

[1] Throughout this paper, charge-conjugate modes are implicitly included unless noted otherwise.

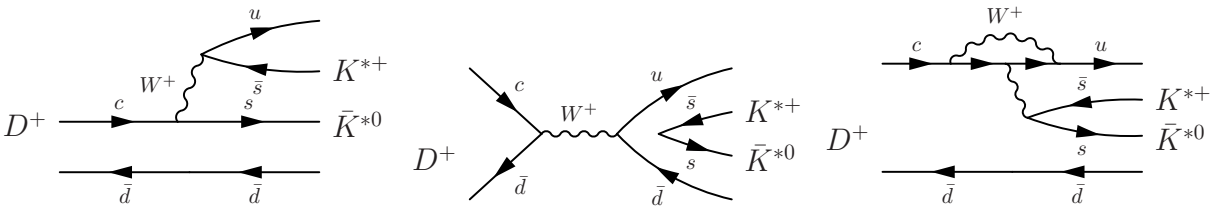

Figure 1: Tree (left), annihilation (center), and "penguin" (right) diagrams contributing to $D^+ \to \overline{K}^{*0}K^{*+}$. This decay is expected to be the dominant process for the four-body decay $D^+ \to K^0_S K^-\pi^+\pi^+$.

2 Methodology

The topology of $D^+_{(s)} \to K^0_S K^-\pi^+\pi^+$ decays is shown in figure 2. The angle in the $D^+_{(s)}$ rest frame between the decay planes of the $K^0_S\pi^+$ pair and the $K^-\pi^+$ pair is denoted φ. Also shown are two helicity angles, $\theta_{K^0_S}$ and θ_{K^-}. These are defined as the angle in the $K^0_S\pi^+$ or $K^-\pi^+$ rest frame between the kaon momentum and the direction opposite that of the $D^+_{(s)}$ momentum.

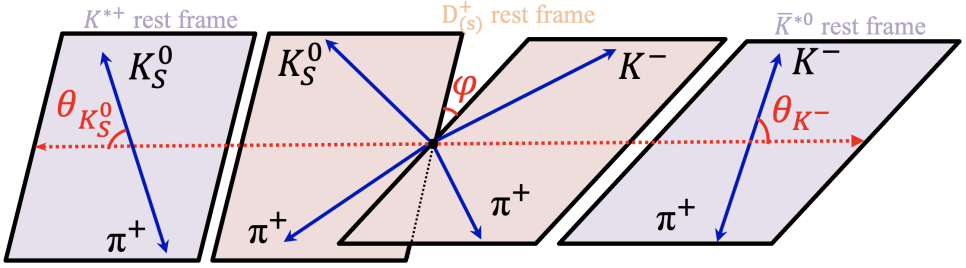

Figure 2: Decay topology for $D^+_{(s)} \to K^0_S K^-\pi^+\pi^+$. The innermost decay planes, as drawn, correspond to the $D^+_{(s)}$ rest frame; the outermost decay planes, as drawn, correspond to the $K^0_S\pi^+$ and $K^-\pi^+$ rest frames.

The triple- and quadruple products are defined as:

$$C_{\rm TP} = (\vec{p}_{K^-} \times \vec{p}_{\pi^+_h}) \cdot \vec{p}_{K^0_S}\,, \quad (1)$$

$$C_{\rm QP} = (\vec{p}_{K^-} \times \vec{p}_{\pi^+_h}) \cdot (\vec{p}_{K^0_S} \times \vec{p}_{\pi^+_l})\,, \quad (2)$$

where the subscripts "h" or "l" denote the pion with the higher or lower momentum, respectively. All momenta are measured in the $D^+_{(s)}$ rest frame [2] In addition to searching for *CPV* using $C_{\rm TP}$ and $C_{\rm QP}$, we also use the product $C_{\rm TP}C_{\rm QP}$ and three functions of the helicity angles: $\cos\theta_{K^0_S}\cos\theta_{K^-}$, $C_{\rm TP}\cos\theta_{K^0_S}\cos\theta_{K^-}$, and $C_{\rm QP}\cos\theta_{K^0_S}\cos\theta_{K^-}$. The observables $C_{\rm QP}$, $C_{\rm TP}$, and $C_{\rm TP}C_{\rm QP}$ have the same signs as $\cos\varphi$, $\sin\varphi$, and $\sin(2\varphi)$,

[2] For $C_{\rm TP}$, the choice of the three out of four final state momenta does not impact the measurement, as the total momentum sums to zero. For $C_{\rm QP}$, the combinations are chosen to be similar to $C_{\rm TP}$.

respectively. The observable $C_{\rm TP}\cos\theta_{K^0_S}\cos\theta_{K^-}$ has the same sign as a term in the angular distribution of $D \to V_a V_b$, $V \to P_1 P_2$ decays [16]: $d^2_{1,0}(\theta_a) d^2_{1,0}(\theta_b)\sin\varphi$, which is proportional to $\sin(2\theta_a)\sin(2\theta_b)\sin\varphi$. The term $C_{\rm QP}\cos\theta_{K^0_S}\cos\theta_{K^-}$ has the same sign as another term, $d^2_{1,0}(\theta_a) d^2_{1,0}(\theta_b)\cos\varphi$, which is proportional to $\sin(2\theta_a)\sin(2\theta_b)\cos\varphi$. In these expressions, V and P denote vector and pseoduscalar mesons, and the d's denote Wigner d functions [19, 20]. We thus measure six observables, $X = C_{\rm TP}$, $C_{\rm QP}$, $C_{\rm TP}C_{\rm QP}$, $\cos\theta_{K^0_S}\cos\theta_{K^-}$, $C_{\rm TP}\cos\theta_{K^0_S}\cos\theta_{K^-}$, and $C_{\rm QP}\cos\theta_{K^0_S}\cos\theta_{K^-}$, the signs of which correspond to the signs of different combinations of $\sin\varphi$, $\cos\varphi$, $\cos\theta_{K^0_S}$, and $\cos\theta_{K^-}$.

For each observable, we measure the asymmetry about zero for both $D^+_{(s)}$ and $D^-_{(s)}$ decays:

$$A_X(D^+_{(s)}) \equiv \frac{N(X>0) - N(X<0)}{N(X>0) + N(X<0)} \tag{3}$$

$$\bar{A}_{\overline{X}}(D^-_{(s)}) \equiv \frac{\overline{N}(\overline{X}>0) - \overline{N}(\overline{X}<0)}{\overline{N}(\overline{X}>0) + \overline{N}(\overline{X}<0)}, \tag{4}$$

where N and $\overline{N}$ denote the yields of $D^+_{(s)}$ and $D^-_{(s)}$ decays, respectively. For the observables proportional to $C_{\rm TP}$, $\overline{X} = -X$ to account for the oddness of $C_{\rm TP}$ under a parity transformation; for the other observables, $\overline{X} = +X$. With this definition, A_X and $\bar{A}_{\overline{X}}$ are CP-conjugate quantities for all the observables, and any difference violates CP. We parameterize a difference with

$$\mathcal{A}^X_{CP} \equiv \frac{A_X - \bar{A}_{\overline{X}}}{2}, \tag{5}$$

where $\mathcal{A}^X_{CP} \neq 0$ indicates CP violation.

3 Detector and data set

The Belle detector [21] was a large-solid-angle spectrometer that operated at the KEKB asymmetric-energy e^+e^- collider [22]. It had a cylindrical geometry and consisted of a silicon vertex detector (SVD), a central drift chamber (CDC), an array of aerogel threshold Cherenkov counters (ACC), a barrel-like arrangement of time-of-flight scintillation counters (TOF), and an electromagnetic calorimeter (ECL) based on CsI(Tl) crystals. These components were located inside a superconducting solenoid coil that provided a 1.5 T magnetic field. The iron flux-return of the magnet was instrumented with resistive-plate chambers (KLM) to detect muons and K^0_L mesons. More details on the Belle detector are provided in refs. [21, 23].

The Belle II detector [24], operates at the SuperKEKB asymmetric-energy e^+e^- collider [25] and also has a cylindrical geometry. It includes a two-layer silicon-pixel detector (PXD) surrounded by a four-layer double-sided silicon-strip detector [26] and a 56-layer central drift chamber. Only one sixth of the second layer of the PXD was installed for the data analyzed here. Surrounding the CDC is a time-of-propagation counter (TOP) [27] in the central region, and an aerogel-based ring-imaging Cherenkov counter (ARICH)

in the forward region. Surrounding the TOP and ARICH is the ECL and the 1.5 T superconducting solenoid magnet previously used in Belle. The magnet's flux return is instrumented with both resistive-plate chambers and plastic scintillator modules to detect muons, K_L^0 mesons, and neutrons. More details on the Belle II detector are provided in ref. [24]. For both Belle and Belle II, the symmetry axis of the detectors, defined as the z axis, is almost coincident with the direction of the electron beam. Both magnetic fields run parallel to the z axis.

This analysis uses both Belle and Belle II data sets, 980 fb^{-1} recorded by Belle and 427 fb^{-1} recorded by Belle II. The majority of the data (73% for Belle, 85% for Belle II) were recorded at an e^+e^- center-of-mass (c.m.) energy corresponding to the $\Upsilon(4S)$ resonance. The remaining data were recorded at energies slightly above and below the $\Upsilon(4S)$ resonance and at other $\Upsilon(nS)$ ($n = 1, 2, 3, 5$) resonances. We use Monte Carlo (MC) simulated events to optimize selection criteria, study backgrounds, and calculate reconstruction efficiencies. The MC samples are generated using EvtGen [28], and the detector response is simulated using Geant3 [28] for Belle and Geant4 [29] for Belle II. The continuum process $e^+e^- \to q\bar{q}$, where $q = u, d, s, c$, is generated using Pythia8 [30] for Belle and Pythia8 [30] and KKMC [31] for Belle II. Final-state radiation of charged particles is simulated with Photos [32].

4 Event selection

The analysis is performed using the Belle II analysis software framework (BASF2) [33]. The Belle data sets are converted to BASF2 format using the B2BII software package [34]. Selection criteria are chosen to maximize a figure-of-merit FOM $= N_S/\sqrt{N_S + N_B}$, where N_S is the signal yield expected in a region $|M(D) - m_D| < 13$ MeV/c^2, and N_B is the background yield expected in this region. Here, $M(D) = M(K_S^0 K^- \pi^+ \pi^+)$ is the invariant mass of the $D_{(s)}^+$ candidate, m_D is the nominal $D_{(s)}^+$ mass [35], and the range corresponds to about 2.5σ in resolution. The background yield is obtained from MC simulation, with a correction factor applied to account for the ratio of yields between data and MC simulation in the sideband 20 MeV/c^2 $< |M(D) - m_D| <$ 40 MeV/c^2.

We require that signal candidates pass the following selection criteria. Charged tracks must lie within the CDC acceptance (an angular coverage of $17° \leq \theta \leq 150°$), have at least one CDC hit, and have a distance-of-closest-approach to the e^+e^- interaction point (IP) of less than 2.0 cm along the z direction and less than 0.5 cm in the x-y (transverse) plane. For each track, we calculate particle identification (PID) likelihoods ($\mathcal{L}$) for π, K, and p particle hypotheses using information from the CDC, ACC, and TOF detectors in Belle, and mainly from the CDC, TOP, and ARICH detectors in Belle II. Tracks satisfying a likelihood ratio $\mathcal{L}_\pi/(\mathcal{L}_\pi + \mathcal{L}_K) > 0.6$ are identified as pions, and tracks satisfying a ratio $\mathcal{L}_K/(\mathcal{L}_K + \mathcal{L}_\pi) > 0.6$ are identified as kaons. Tracks that are highly electron-like or muon-like are rejected, where the electron and muon likelihoods are determined mainly using information from the ECL and KLM detectors, respectively [36–38]. These requirements have an average efficiency of 91% for kaons and 95% for pions at Belle, and 87% for kaons and 90% for pions at Belle II.

Candidate K_S^0 mesons are reconstructed from pairs of oppositely-charged tracks as-

sumed to be pions. To suppress non-K^0_S background at Belle, a neural network (NN) [39] is employed. This NN uses 13 input variables [40]; the most discriminating are the K^0_S momentum in the laboratory frame, the distance to the IP in the x-y plane for each track, and the K^0_S flight length in the x-y plane. To suppress non-K^0_S background at Belle II, the pion candidates are required to originate from a common vertex with a fit quality $\chi^2(K^0_S) < 100$. For both Belle and Belle II, the K^0_S flight length (L) is calculated as the projection of the displacement vector joining the K^0_S production and decay vertices onto the direction of the K^0_S momentum. The uncertainty σ_L is calculated by propagating the uncertainties on the vertex positions and the K^0_S momentum, accounting for their correlations. The K^0_S flight significance, L/σ_L, is required to be greater than 10 at Belle and greater than 20 at Belle II. The invariant mass of the $K^0_S \to \pi^+\pi^-$ candidate is required to lie within 10 MeV/c^2 of the nominal K^0_S mass [35]. The efficiencies of these requirements is about 97% at Belle and 92% at Belle II.

We reconstruct $D^+_{(s)}$ candidates by combining a K^0_S candidate, a K^- track, and two π^+ tracks. A vertex fitting algorithm [41] is applied to the entire decay chain, subject to a mass constraint for the K^0_S and a constraint that the $D^+_{(s)}$ momentum originate from the IP. The resulting goodness-of-fit χ^2 is required to be less than 30 for D^+ decays and less than 40 for D^+_s decays. The $D^+_{(s)}$ flight significance, defined as L_D/σ_{L_D}, is required to be greater than 3.0 (0.5) for D^+ (D^+_s) decays at Belle, and greater than 4.5 (2.0) for D^+ (D^+_s) decays at Belle II. The tighter criteria for Belle II results from the superior vertex resolution of the Belle II PXD detector and has similar efficiency as the Belle criteria.

We define a scaled momentum for the $D^+_{(s)}$ candidate as $x_p \equiv p_D/p_{\rm max}$, where p_D is the D momentum and $p_{\rm max} = \sqrt{E^2_{\rm beam} - M(D)^2c^4}/c$. Here, $E_{\rm beam}$ is the beam energy, and both $E_{\rm beam}$ and p_D are evaluated in the e^+e^- center-of-mass frame. To suppress $D^+_{(s)}$ decays originating from B decays and also combinatorial background, we require $x_p > 0.5$. We also require that the invariant mass of the $D^+_{(s)}$ candidate satisfy $\big[M(D) - m_D\big] \in (-50, 40)$ MeV/c^2. For D^+_s candidates, an additional background arising from $D^{*+} \to D^0(\to K^0_S K^-\pi^+)\pi^+$ is present in the upper $M(K^0_S K^-\pi^+\pi^+)$ sideband. To suppress this background, we require that, for each π^+ candidate, $\big[M(K^0_S K^-\pi^+\pi^+) - M(K^0_S K^-\pi^+)\big] > 151.57$ MeV/c^2. This requirement eliminates essentially all such background while preserving more than 99% of signal decays.

5 $\mathcal{A}^X_{CP}$ measurement

We measure the asymmetries $\mathcal{A}^X_{CP}$ in two steps. We first perform a fit to the $M(D)$ distributions of combined samples of $(D^+ + D^-)$ and $(D^+_s + D^-_s)$ decays. The probability density function (PDF) for signal decays is taken to be the sum of a double Gaussian and two (for D^+) or three (for D^+_s) asymmetric Gaussians. These functions share a common mean parameter but have distinct width parameters. These parameters are taken from MC simulation, but a shift δ_μ to the mean and a common scaling factor k_σ for the widths are included to account for small differences between data and MC simulation. The PDF for background is taken to be a straight line: $f(x) = 1 + \alpha\, x$.

The combined data sets and projections of the fit result are shown in figure 3. The

resulting signal and background yields are listed in table 1. The ratio of signal to background for Belle II is higher than that for Belle due to the improved resolution on the $D^+_{(s)}$ flight length L_D.

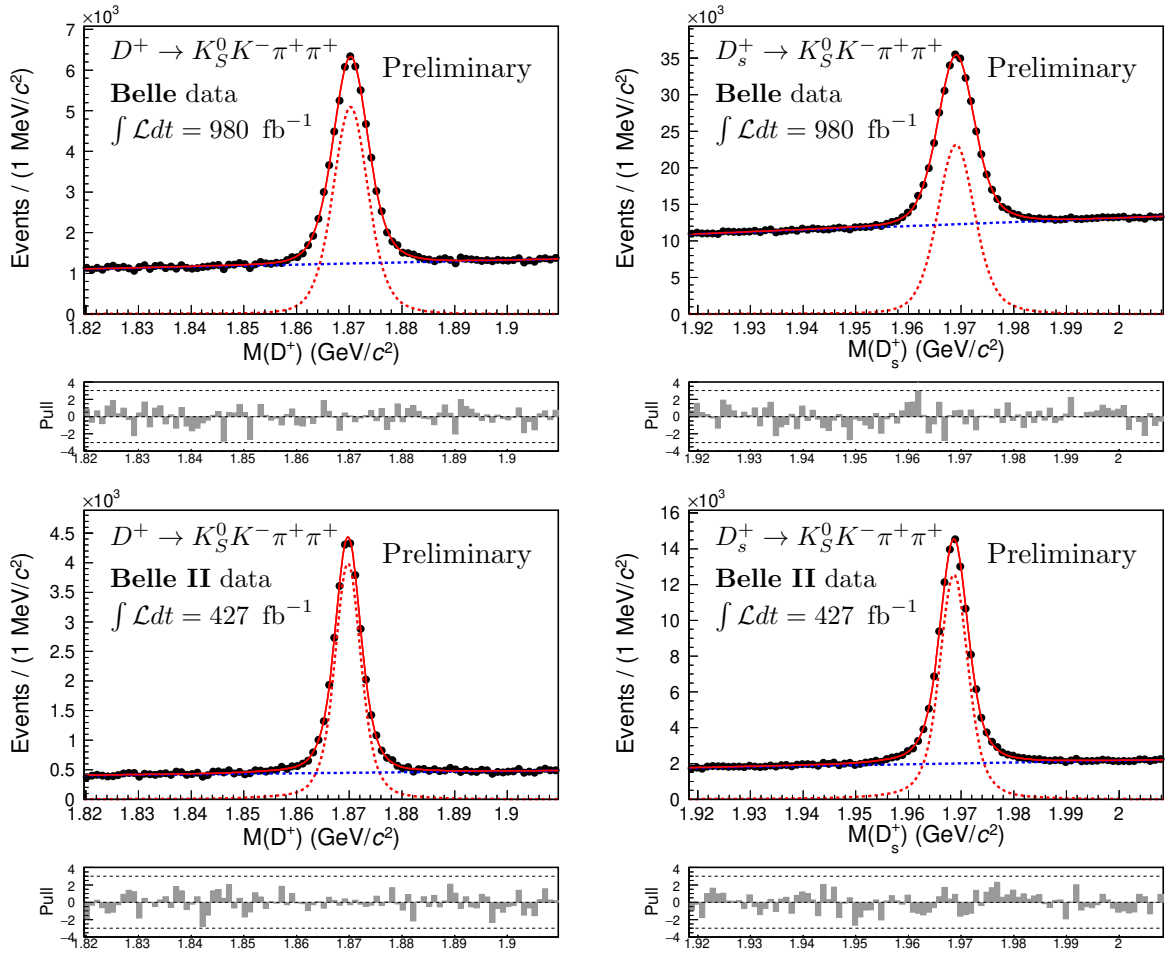

Figure 3: Invariant mass distributons for $D^+_{(s)} \to K^0_S K^-\pi^+\pi^+$ candidates (points with error bars), along with projections of the fit result. The red dashed curves show the fitted signal, and the blue dash-dotted curves show the fitted background. The top plots show Belle data, and the bottom plots show Belle II data. The smaller plots show the corresponding pull distributions, where the pull is defined as (fitted yield − actual yield)/(fitted uncertainty).

Subsequently, we perform a second fit for the asymmetries $\mathcal{A}^X_{CP}$, where the calibration factors δ_μ, k_σ, and slope α are fixed to the values obtained from the first fit. For the $\mathcal{A}^X_{CP}$ fit, we divide the data into four X subsamples as determined by the charge of $D^\pm_{(s)}$ and

Table 1: Fitted yields of signal and background at Belle and Belle II.

Component	$D^+ \to K^0_S K^-\pi^+\pi^+$		$D^+_s \to K^0_S K^-\pi^+\pi^+$	
	Belle	Belle II	Belle	Belle II
Signal ($N_{\rm sig}$)	46073 ± 301	28224 ± 209	223182 ± 826	98214 ± 419
Background ($N_{\rm bkg}$)	110555 ± 394	39937 ± 236	1091491 ± 1245	177743 ± 505
Ratio ($N_{\rm sig}/N_{\rm bkg}$)	0.42	0.71	0.20	0.55

the sign of X. The yields of the subsamples are expressed as:

$$N(D^+_{(s)}, X>0) = \frac{N_+}{2}(1+A_X) \quad (6)$$

$$N(D^+_{(s)}, X<0) = \frac{N_+}{2}(1-A_X) \quad (7)$$

$$N(D^-_{(s)}, \overline{X}>0) = \frac{N_-}{2}(1+A_X-2\mathcal{A}^X_{CP}) \quad (8)$$

$$N(D^-_{(s)}, \overline{X}<0) = \frac{N_-}{2}(1-A_X+2\mathcal{A}^X_{CP})\,. \quad (9)$$

Here, N_+ and N_- represent signal yields for $D^+_{(s)}$ and $D^-_{(s)}$, respectively; A_X denotes the asymmetry for X; and $\mathcal{A}^X_{CP}$ denotes the CP-violating parameter. We perform a simultaneous fit to the $M(D)$ distributions of these four subsamples to extract parameters N_+, N_-, A_X, and $\mathcal{A}^X_{CP}$. We test the fitting procedure on MC samples generated with different input values of $\mathcal{A}^X_{CP}$; in all cases we obtain fitted values for $\mathcal{A}^X_{CP}$ consistent with the input values.

The fitted $M(D)$ distributions for Belle and Belle II data are shown in appendix A. The results for $\mathcal{A}^X_{CP}$ are listed in table 2 along with systematic uncertainties; these uncertainties are discussed in the next section.

6 Systematic uncertainties

Many systematic uncertainties for the measurements of X and $\overline{X}$ cancel in the ratios A_X (eq. 3) and $\bar{A}_{\overline{X}}$ (eq. 4), or in the difference between them (eq. 5). The uncertainties that do not cancel are listed in table 3 and discussed below.

A possible difference in efficiency between $+X$ and $-X$ values is evaluated using MC simulation by comparing reconstructed X distributions with those that were generated. For $X = C_{\rm TP}$ and $C_{\rm TP}C_{\rm QP}$, no significant X-dependence is observed, i.e., the ratio of distributions for reconstructed and generated events is nearly flat. For the other observables, the ratio is not flat, but the observed dependence is the same for $D^+_{(s)}$ and $D^-_{(s)}$ decays and thus the effect upon $\mathcal{A}^X_{CP}$ is small. To account for this quantitatively, we take as a systematic uncertainty the difference between generated and reconstructed values of $\mathcal{A}^X_{CP}$. We include in this uncertainty that arising from the limited statistics of the MC samples used. Finally, we include in this uncertainty any effect upon $\mathcal{A}^X_{CP}$ arising from a possible

Table 2: Results for $\mathcal{A}_{CP}^{X}$ in $D_{(s)}^{+} \to K_S^0 K^- \pi^+ \pi^+$ decays, where $X = C_{\rm TP}$ (1), $C_{\rm QP}$ (2), $C_{\rm TP}C_{\rm QP}$ (3), $\cos\theta_{K_S^0}\cos\theta_{K^-}$ (4), $C_{\rm TP}\cos\theta_{K_S^0}\cos\theta_{K^-}$ (5), and $C_{\rm QP}\cos\theta_{K_S^0}\cos\theta_{K^-}$ (6). The significance of the combined $\mathcal{A}_{CP}^{X}$ result from $\mathcal{A}_{CP}^{X} = 0$ is listed in the last column.

Decay	X	$\mathcal{A}_{CP}^{X}$ (10^{-3}) at Belle	$\mathcal{A}_{CP}^{X}$ (10^{-3}) at Belle II	Combined $\mathcal{A}_{CP}^{X}$ (10^{-3})	Significance
D^+	(1)	$-4.0 \pm 5.9 \pm 3.0$	$-0.2 \pm 7.0 \pm 1.8$	$-2.3 \pm 4.5 \pm 1.5$	0.5σ
	(2)	$-1.0 \pm 5.9 \pm 2.5$	$-0.4 \pm 7.0 \pm 2.4$	$-0.7 \pm 4.5 \pm 1.7$	0.2σ
	(3)	$+6.4 \pm 5.9 \pm 2.2$	$+0.6 \pm 7.0 \pm 1.3$	$+3.9 \pm 4.5 \pm 1.1$	0.8σ
	(4)	$-4.7 \pm 5.9 \pm 3.0$	$-0.6 \pm 6.9 \pm 3.0$	$-2.9 \pm 4.5 \pm 2.1$	0.6σ
	(5)	$+1.9 \pm 5.9 \pm 2.0$	$-0.2 \pm 7.0 \pm 1.9$	$+1.0 \pm 4.5 \pm 1.4$	0.2σ
	(6)	$+14.9 \pm 5.9 \pm 1.4$	$+7.0 \pm 7.0 \pm 1.6$	$+11.6 \pm 4.5 \pm 1.1$	2.5σ
D_s^+	(1)	$-0.3 \pm 3.1 \pm 1.3$	$+1.0 \pm 3.9 \pm 1.1$	$+0.2 \pm 2.4 \pm 0.8$	0.1σ
	(2)	$+0.6 \pm 3.1 \pm 1.2$	$+2.0 \pm 3.9 \pm 1.4$	$+1.1 \pm 2.4 \pm 0.9$	0.4σ
	(3)	$+1.5 \pm 3.2 \pm 1.4$	$-2.7 \pm 3.9 \pm 1.7$	$-0.2 \pm 2.5 \pm 1.1$	0.1σ
	(4)	$-3.7 \pm 3.1 \pm 1.1$	$-6.3 \pm 3.9 \pm 1.2$	$-4.7 \pm 2.4 \pm 0.8$	1.8σ
	(5)	$-4.4 \pm 3.2 \pm 1.4$	$+0.8 \pm 3.9 \pm 1.4$	$-2.2 \pm 2.5 \pm 1.0$	0.8σ
	(6)	$-1.6 \pm 3.1 \pm 1.3$	$-0.0 \pm 3.9 \pm 1.7$	$-1.0 \pm 2.4 \pm 1.0$	0.4σ

Table 3: Systematic uncertainties (absolute) for $\mathcal{A}_{CP}^{X}$ in units of 10^{-3} in $D_{(s)}^{+} \to K_S^0 K^- \pi^+ \pi^+$ decays, where $X = C_{\rm TP}$ (1), $C_{\rm QP}$ (2), $C_{\rm TP}C_{\rm QP}$ (3), $\cos\theta_{K_S^0}\cos\theta_{K^-}$ (4), $C_{\rm TP}\cos\theta_{K_S^0}\cos\theta_{K^-}$ (5), and $C_{\rm QP}\cos\theta_{K_S^0}\cos\theta_{K^-}$ (6).

Source	$D^+ \to K_S^0 K^- \pi^+ \pi^+$ at Belle						$D^+ \to K_S^0 K^- \pi^+ \pi^+$ at Belle II					
	(1)	(2)	(3)	(4)	(5)	(6)	(1)	(2)	(3)	(4)	(5)	(6)
X-dependent efficiency	3.0	2.4	1.9	2.8	1.8	1.4	1.2	2.4	1.1	2.6	1.5	1.3
X-resolution asymmetry	0.2	0.7	0.4	0.7	0.6	0.3	0.7	0.1	0.1	0.9	0.2	0.7
Signal/background PDF	0.0	0.0	0.0	0.0	0.0	0.0	0.0	0.0	0.0	0.0	0.0	0.0
Simultaneous fit bias	0.2	0.2	0.1	0.2	0.1	0.2	0.2	0.2	0.2	0.1	0.2	0.2
D_s^+ feeddown background	0.4	0.3	1.0	0.7	0.1	0.2	1.1	0.4	0.6	1.1	1.2	0.6
Total $\sigma_{\rm syst}$	3.0	2.5	2.2	3.0	2.0	1.4	1.8	2.4	1.3	3.0	1.9	1.6
Source	$D_s^+ \to K_S^0 K^- \pi^+ \pi^+$ at Belle						$D_s^+ \to K_S^0 K^- \pi^+ \pi^+$ at Belle II					
	(1)	(2)	(3)	(4)	(5)	(6)	(1)	(2)	(3)	(4)	(5)	(6)
X-dependent efficiency	1.2	1.1	1.4	1.1	1.2	1.3	1.1	1.4	1.7	1.2	1.4	1.6
X-resolution asymmetry	0.6	0.5	0.1	0.2	0.8	0.3	0.2	0.1	0.2	0.0	0.2	0.4
Signal/background PDF	0.0	0.0	0.0	0.0	0.0	0.0	0.0	0.0	0.0	0.0	0.0	0.0
Simultaneous fit bias	0.1	0.0	0.0	0.1	0.1	0.0	0.1	0.2	0.2	0.3	0.2	0.2
Total $\sigma_{\rm syst}$	1.3	1.2	1.4	1.1	1.4	1.3	1.1	1.4	1.7	1.2	1.4	1.7

difference between MC simulation and data for X-dependent efficiencies. We evaluate this as follows. The asymmmetry in detection efficiencies between K^+ and K^- (denoted A_ε^K) is measured in data as a function of momentum and polar angle using $D^0 \to K^-\pi^+$ and $D_s^+ \to \phi\pi^+$ decays [42], and the asymmetry in detection efficiencies between π^+ and π^- (denoted A_ε^π) is measured using $D^+ \to K^-\pi^+\pi^+$ and $D^0 \to K^-\pi^+\pi^0$ decays [43]. We scale MC signal events by weighting factors based on these asymmetries and repeat the fits for $\mathcal{A}_{CP}^X$. For $D_{(s)}^+ \to K_S^0 K^-\pi^+\pi^+$, the weighting factor is $(1-A_\varepsilon^K)(1+A_\varepsilon^\pi)(1+A_\varepsilon^\pi)$; for $D_{(s)}^- \to K_S^0 K^+\pi^-\pi^-$, the weighting factor is $(1+A_\varepsilon^K)(1-A_\varepsilon^\pi)(1-A_\varepsilon^\pi)$. After fitting these reweighted events, the resulting change in $\mathcal{A}_{CP}^X$ is included in the systematic uncertainty for X-dependent efficiency. This contribution is very small ($< 5 \times 10^{-4}$).

We consider the effect of a difference in X *resolution* between positive and negative values. If such a difference existed, then a different number of events could shift from $-X$ to $+X$ values than from $+X$ to $-X$, thus corrupting the A_X asymmetry. From MC simulation, we find that the net fraction of signal decays changing sign in X is very small, less than 0.1%. To evaluate the effect quantitatively, we study the X resolution for different ranges of X. We find the resolution in X to depend on X but be well-described by a parabola symmetric about $X = 0$. The statistical error on this asymmetry is used to generate MC samples with asymmetric resolution; these samples are then fitted and the resulting change in $\mathcal{A}_{CP}^X$ is taken as the systematic uncertainty due to a possible asymmetry in X resolution.

The uncertainty due to fixed PDF shape parameters is evaluated by varying these parameters by their uncertainties and repeating the fit. We sample all parameters simultaneously from Gaussian distributions having widths equal to their uncertainties, and repeat this sampling and subsequent fitting 1000 times. During this sampling, correlations among the sampled parameters are accounted for. The 1000 fitted values for $\mathcal{A}_{CP}^X$ are recorded, and the root-mean-square (r.m.s.) of this distribution is taken as the systematic uncertainty due to signal and background PDF shapes. These r.m.s. values are tiny, less than 2×10^{-5}.

To assess possible small bias in our fitting procedure, we fit a large sample of "toy" MC events that are generated by sampling from the PDFs used to fit the data. The number of generated events for $\pm X$ and $\pm\overline{X}$ vary: they are calculated for different input values of $\mathcal{A}_{CP}^X$, which range from -0.015 to 0.015. For each input value, an ensemble of MC events is generated. These ensembles are fitted, and the mean value of the $\mathcal{A}_{CP}^X$ results is calculated. Plotting these mean values against the input values shows a linear dependence. Fitting these points to a line gives a slope consistent with unity and an intercept consistent with zero. We assign the difference between our measured value and the input value corresponding to the measured value (as given by the fitted line) as a systematic uncertainty due to possible fit bias. The uncertainty on the difference is included in this calculation.

For the $D^+ \to K_S^0 K^-\pi^+\pi^+$ decay mode, we consider the effect of possible background from $D_s^+ \to K_S^0 K^-\pi^+\pi^+\pi^0$, with the π^0 missed. This five-body decay is unmeasured, and thus to evaluate the effect of this background, we include a component for it in our fit. We take the shape of its PDF from MC simulation and float its yield. The difference between the resulting value of $\mathcal{A}_{CP}^X$ and our nominal result is taken as a systematic uncertainty.

Combining all systematic uncertainties in quadrature gives the total systematic uncer-

tainties listed in table 3. These total uncertainties are also included in table 2. For all $\mathcal{A}_{CP}^{X}$ measurements, the total systematic uncertainties are notably less than the corresponding statistical uncertainties.

7 Combined result and summary

Table 2 lists our results for the six asymmetries $\mathcal{A}_{CP}^{X}$, for both Belle and Belle II. We combine the results from the two data sets using the formulae

$$\mathcal{A}_{CP}^{X} = \frac{\mathcal{A}_{CP}^{B1}/\sigma_{B1}^2 + \mathcal{A}_{CP}^{B2}/\sigma_{B2}^2}{1/\sigma_{B1}^2 + 1/\sigma_{B2}^2} \tag{10}$$

$$\sigma_{\mathcal{A}_{CP}^{X}} = \frac{1}{\sqrt{1/\sigma_{B1}^2 + 1/\sigma_{B2}^2}}\,, \tag{11}$$

where σ_{B_1} and σ_{B_2} represent the total uncertainties (sum in quadrature of statistical and systematic uncertainties) for Belle and Belle II measurements, respectively. The combined results are also listed in table 2; the resulting uncertainties are 0.5% for D^+ decays and less than 0.3% for D_s^+ decays. We calculate the significance of the combined results from the null hypothesis ($\mathcal{A}_{CP}^{X} = 0$) by dividing the central values by their total uncertainties. These significances are listed in the right-most column of table 2 and are mostly less than 1σ. The largest significance (for D^+ $X = C_{\rm QP}\cos\theta_{K_S^0}\cos\theta_{K^-}$) is 2.5σ, which for 12 measurements is plausible as a statistical fluctuation.

In summary, we have performed a first search for *CP* violation in four-body $D_{(s)}^+ \to K_S^0 K^-\pi^+\pi^+$ decays. We use both Belle and Belle II datasets corresponding to a total integrated luminosity of 1407 fb^{-1}. We have measured *CP* asymmetries for six different observables consisting of the triple product $C_{\rm TP}$, the quadruple product $C_{\rm QP}$, the product $C_{\rm TP}C_{\rm QP}$, the product of the cosines of helicity angles $\theta_{K_S^0}$ and θ_{K^-}, and the products of $C_{\rm TP}$ and $C_{\rm QP}$ with the product $\cos\theta_{K_S^0}\cos\theta_{K^-}$. All results are listed in table 2. No evidence for *CP* violation is found. These results represent the world's most precise measurements of the triple-product asymmetry for D_s^+ decays and for SCS D^+ decays, and the first use of the other $\mathcal{A}_{CP}^{X}$ asymmetries to search for *CP* violation in the charm sector.

Acknowledgements

The Belle collaboration thanks the SuperKEKB team for delivering high-luminosity collisions; the KEK cryogenics group for the efficient operation of the detector solenoid magnet; the KEK computer group and the NII for on-site computing support and SINET6 network support; and the raw-data centers at BNL, DESY, GridKa, IN2P3, INFN, and the University of Victoria for offsite computing support.

The Belle II collaboration is grateful for support from the Science Committee of the Republic of Armenia Grant No. 20TTCG-1C010; Australian Research Council and research Grants No. DE220100462, No. DP180102629, No. DP170102389, No. DP170102204, No. DP150103061, No. FT130100303, No. FT130100018, and No. FT120100745; Austrian Federal Ministry of

Education, Science and Research, Austrian Science Fund No. P 31361-N36 and No. J4625-N, and Horizon 2020 ERC Starting Grant No. 947006 “InterLeptons”; Natural Sciences and Engineering Research Council of Canada, Compute Canada and CANARIE; Chinese Academy of Sciences and research Grant No. QYZDJ-SSW-SLH011, National Natural Science Foundation of China and research Grants No. 11521505, No. 11575017, No. 11675166, No. 11761141009, No. 11705209, and No. 11975076, LiaoNing Revitalization Talents Program under Contract No. XLYC1807135, Shanghai Pujiang Program under Grant No. 18PJ1401000, Shandong Provincial Natural Science Foundation Project ZR2022JQ02, and the CAS Center for Excellence in Particle Physics (CCEPP); the Ministry of Education, Youth, and Sports of the Czech Republic under Contract No. LTT17020 and Charles University Grant No. SVV 260448 and the Czech Science Foundation Grant No. 22-18469S; European Research Council, Seventh Framework PIEF-GA-2013-622527, Horizon 2020 ERC-Advanced Grants No. 267104 and No. 884719, Horizon 2020 ERC-Consolidator Grant No. 819127, Horizon 2020 Marie Sklodowska-Curie Grant Agreement No. 700525 ”NIOBE” and No. 101026516, and Horizon 2020 Marie Sklodowska-Curie RISE project JENNIFER2 Grant Agreement No. 822070 (European grants); L’Institut National de Physique Nucléaire et de Physique des Particules (IN2P3) du CNRS (France); BMBF, DFG, HGF, MPG, and AvH Foundation (Germany); Department of Atomic Energy under Project Identification No. RTI 4002 and Department of Science and Technology (India); Israel Science Foundation Grant No. 2476/17, U.S.-Israel Binational Science Foundation Grant No. 2016113, and Israel Ministry of Science Grant No. 3-16543; Istituto Nazionale di Fisica Nucleare and the research grants BELLE2; Japan Society for the Promotion of Science, Grant-in-Aid for Scientific Research Grants No. 16H03968, No. 16H03993, No. 16H06492, No. 16K05323, No. 17H01133, No. 17H05405, No. 18K03621, No. 18H03710, No. 18H05226, No. 19H00682, No. 22H00144, No. 26220706, and No. 26400255, the National Institute of Informatics, and Science Information NETwork 5 (SINET5), and the Ministry of Education, Culture, Sports, Science, and Technology (MEXT) of Japan; National Research Foundation (NRF) of Korea Grants No. 2016R1D1A1B02012900, No. 2018R1-A2B3003643, No. 2018R1A6A1A06024970, No. 2018R1D1A1B07047294, No. 2019R1-I1A3A01058933, No. 2022R1A2C1003993, and No. RS-2022-00197659, Radiation Science Research Institute, Foreign Large-size Research Facility Application Supporting project, the Global Science Experimental Data Hub Center of the Korea Institute of Science and Technology Information and KREONET/GLORIAD; Universiti Malaya RU grant, Akademi Sains Malaysia, and Ministry of Education Malaysia; Frontiers of Science Program Contracts No. FOINS-296, No. CB-221329, No. CB-236394, No. CB-254409, and No. CB-180023, and No. SEP-CINVESTAV research Grant No. 237 (Mexico); the Polish Ministry of Science and Higher Education and the National Science Center; the Ministry of Science and Higher Education of the Russian Federation, Agreement No. 14.W03.31.0026, and the HSE University Basic Research Program, Moscow; University of Tabuk research Grants No. S-0256-1438 and No. S-0280-1439 (Saudi Arabia); Slovenian Research Agency and research Grants No. J1-9124 and No. P1-0135; Agencia Estatal de Investigacion, Spain Grant No. RYC2020-029875-I and Generalitat Valenciana, Spain Grant No. CIDEGENT/2018/020 Ministry of Science and Technology and research Grants No. MOST106-2112-M-002-005-MY3 and No. MOST107-2119-M-002-035-MY3, and the Ministry of Education (Taiwan); Thailand Center of Excellence in Physics; TUBITAK ULAKBIM (Turkey);

National Research Foundation of Ukraine, project No. 2020.02/0257, and Ministry of Education and Science of Ukraine; the U.S. National Science Foundation and research Grants No. PHY-1913789 and No. PHY-2111604, and the U.S. Department of Energy and research Awards No. DE-AC06-76RLO1830, No. DE-SC0007983, No. DE-SC0009824, No. DE-SC0009973, No. DE-SC0010007, No. DE-SC0010073, No. DE-SC0010118, No. DE-SC0010504, No. DE-SC0011784, No. DE-SC0012704, No. DE-SC0019230, No. DE-SC0021274, No. DE-SC0022350; and the Vietnam Academy of Science and Technology (VAST) under Grant No. DL0000.05/21-23. L. K. Li is grateful to Z. H. Zhang (USC) and F. S. Yu (LZU) for valuable discussions on the *CPV* search method used in this paper.

These acknowledgements are not to be interpreted as an endorsement of any statement made by any of our institutes, funding agencies, governments, or their representatives.

References

[1] A. D. Sakharov,
Violation of *CP* Invariance, *C* asymmetry, and baryon asymmetry of the universe,
Pisma Zh. Eksp. Teor. Fiz. **5** (1967) 32.

[2] M. Kobayashi and T. Maskawa,
CP violation in the renormalizable theory of weak interaction, Prog. Theor. Phys. **49** (1973) 652.

[3] J. Brod, A. L. Kagan, and J. Zupan,
Size of direct *CP* violation in singly Cabibbo-suppressed *D* decays, Phys. Rev. D **86** (2012) 014023, arXiv:1111.5000.

[4] H.-Y. Cheng and C.-W. Chiang,
Revisiting *CP* violation in $D \to PP$ and VP decays, Phys. Rev. D **100** (2019) 093002, arXiv:1909.03063.

[5] H.-Y. Cheng and C.-W. Chiang,
CP violation in quasi-two-body $D \to VP$ decays and three-body *D* decays mediated by vector res
Phys. Rev. D **104** (2021) 073003, arXiv:2104.13548.

[6] A. Dery and Y. Nir,
Implications of the LHCb discovery of *CP* violation in charm decays, JHEP **12** (2019) 104, arXiv:1909.11242.

[7] D. Delepine, G. Faisel, and C. A. Ramirez,
Direct *CP* violation in $D^+ \to K^0(\bar{K}^0)\pi^+$ decays as a probe for new physics, Eur. Phys. J. C **80** (2020) 596, arXiv:1903.02422.

[8] M. Chala, A. Lenz, A. V. Rusov, and J. Scholtz,
ΔA_{CP} within the Standard Model and beyond, JHEP **07** (2019) 161, arXiv:1903.10490.

[9] M. Saur and F.-S. Yu, Charm CPV: observation and prospects, Sci. Bull. **65** (2020) 1428, arXiv:2002.12088.

[10] HFLAV, Y. S. Amhis et al.,
Averages of b-hadron, c-hadron, and τ-lepton properties as of 2021, Phys. Rev. D **107** (2023) 052008, arXiv:2206.07501.

[11] LHCb Collaboration, R. Aaij et al., Observation of *CP* Violation in Charm Decays, Phys. Rev. Lett. **122** (2019) 211803, arXiv:1903.08726.

[12] G. Valencia, Angular Correlations in the Decay $B \to VV$ and CP Violation, Phys. Rev. D **39** (1989) 3339.

[13] A. Datta and D. London,
Triple-product correlations in $B \to V_1 V_2$ decays and new physics, Int. J. Mod. Phys. A **19** (2004) 2505, arXiv:hep-ph/0303159.

[14] J.-P. Wang, Q. Qin, and F.-S. Yu,
CP violation induced by T-odd correlations and its baryonic application, arXiv:2211.07332.

[15] F-S. Yu, *CPV in charmed baryons (theory)*, talk at the 12th International Workshop on CKM unitarity (CKM 2023), 18-22 Sep 2023, Santiago de Compostela, Spain.

[16] G. Durieux and Y. Grossman,
Probing *CP* violation systematically in differential distributions, Phys. Rev. D **92** (2015) 076013, arXiv:1508.03054.

[17] G. Durieux, *CP* violation in multibody decays of beauty baryons, JHEP **10** (2016) 005, arXiv:1608.03288.

[18] Z.-H. Zhang,
Searching for *CP* violation through two-dimensional angular distributions in four-body decays of
Phys. Rev. D **107** (2023) L011301, arXiv:2209.13196.

[19] M. Jacob and G. C. Wick,
On the General Theory of Collisions for Particles with Spin, Annals Phys. **7** (1959) 404.

[20] S. U. Chung, A General formulation of covariant helicity coupling amplitudes, Phys. Rev. D **57** (1998) 431.

[21] A. Abashian et al., The Belle detector, Nucl. Instr. and Meth. A **479** (2002) 117, Detectors for Asymmetric B-factories.

[22] S. Kurokawa and E. Kikutani, Overview of the KEKB accelerators, Nucl. Instr. and Meth. A **499** (2003) 1, KEK-B: The KEK B-factory.

[23] Belle Collaboration, J. Brodzicka et al.,
Physics achievements from the Belle experiment, Prog. Theor. Exp. Phys. **2012** (2012) 04D001.

[24] Belle II Collaboration, T. Abe, Belle II technical design report, arXiv:1011.0352.

[25] K. Akai, K. Furukawa, and H. Koiso, SuperKEKB collider, Nucl. Instrum. Meth. **A907** (2018) 188, arXiv:1809.01958.

[26] Belle-II SVD Group, K. Adamczyk et al.,
The design, construction, operation and performance of the Belle II silicon vertex detector, JINST **17** (2022) P11042, arXiv:2201.09824.

[27] D. Kotchetkov et al.,
Front-end electronic readout system for the Belle II imaging Time-Of-Propagation detector, Nucl. Instrum. Meth. A **941** (2019) 162342, arXiv:1804.10782.

[28] D. J. Lange, The EvtGen particle decay simulation package, Nucl. Instrum. Meth. **A462** (2001) 152.

[29] GEANT4 Collaboration, S. Agostinelli et al., GEANT4–a simulation toolkit, Nucl. Instrum. Meth. A **506** (2003) 250.

[30] T. Sjöstrand et al., An Introduction to PYTHIA 8.2, Comput. Phys. Commun. **191** (2015) 159, arXiv:1410.3012.

[31] S. Jadach, B. F. L. Ward, and Z. Wąs,
The precision Monte Carlo event generator KK for two-fermion final states in e^+e^- collisions, Comput. Phys. Commun. **130** (2000) 260, arXiv:hep-ph/9912214.

[32] E. Barberio, B. van Eijk, and Z. Wąs,
PHOTOS: A universal Monte Carlo for QED radiative corrections in decays, Comput. Phys. Commun. **66** (1991) 115.

[33] Belle II Framework Software Group, T. Kuhr et al., The Belle II Core Software, Comput. Softw. Big Sci. **3** (2019) 1, arXiv:1809.04299.

[34] M. Gelb et al., B2BII: Data Conversion from Belle to Belle II, Comput. Softw. Big Sci. **2** (2018) 9, arXiv:1810.00019.

[35] Particle Data Group, R. L. Workman et al., Review of Particle Physics, Prog. Theor. Exp. Phys. **2022** (2022) 083C01.

[36] K. Hanagaki et al., Electron identification in Belle, Nucl. Instrum. Meth. A **485** (2002) 490, arXiv:hep-ex/0108044.

[37] A. Abashian et al., Muon identification in the Belle experiment at KEKB, Nucl. Instrum. Meth. A **491** (2002) 69.

[38] M. Milesi, J. Tan, and P. Urquijo,
Lepton identification in Belle II using observables from the electromagnetic calorimeter and precis
EPJ Web Conf. **245** (2020) 06023.

[39] M. Feindt and U. Kerzel, The NeuroBayes neural network package, Nucl. Instrum. Meth. A **559** (2006) 190.

[40] Belle Collaboration, H. Nakano et al.,
Measurement of time-dependent *CP* asymmetries in $B^0 \to K^0_S\eta\gamma$ decays, Phys. Rev. D **97** (2018) 092003, arXiv:1803.07774.

[41] Belle II Analysis Software Group, J.-F. Krohn et al.,
Global decay chain vertex fitting at Belle II, Nucl. Instrum. Meth. **A976** (2020) 164269, arXiv:1901.11198.

[42] Belle Collaboration, B. R. Ko et al.,
Search for *CP* Violation in the Decay $D^+ \to K^0_S K^+$, JHEP **02** (2013) 098, arXiv:1212.6112.

[43] Belle Collaboration, B. R. Ko et al.,
Evidence for *CP* Violation in the Decay $D^+ \to K^0_S\pi^+$, Phys. Rev. Lett. **109** (2012) 021601, arXiv:1203.6409, [Erratum: Phys.Rev.Lett. 109, 119903 (2012)].

A Simultaneously fitted distributions for $D^+_{(s)}$ data

The fitted $M(D)$ distributions for Belle data along with projections of the fit result are shown in figures 4 (D^+) and 5 (D_s^+). The corresponding distributions for Belle II data are shown in figures 6 (D^+) and 7 (D_s^+).

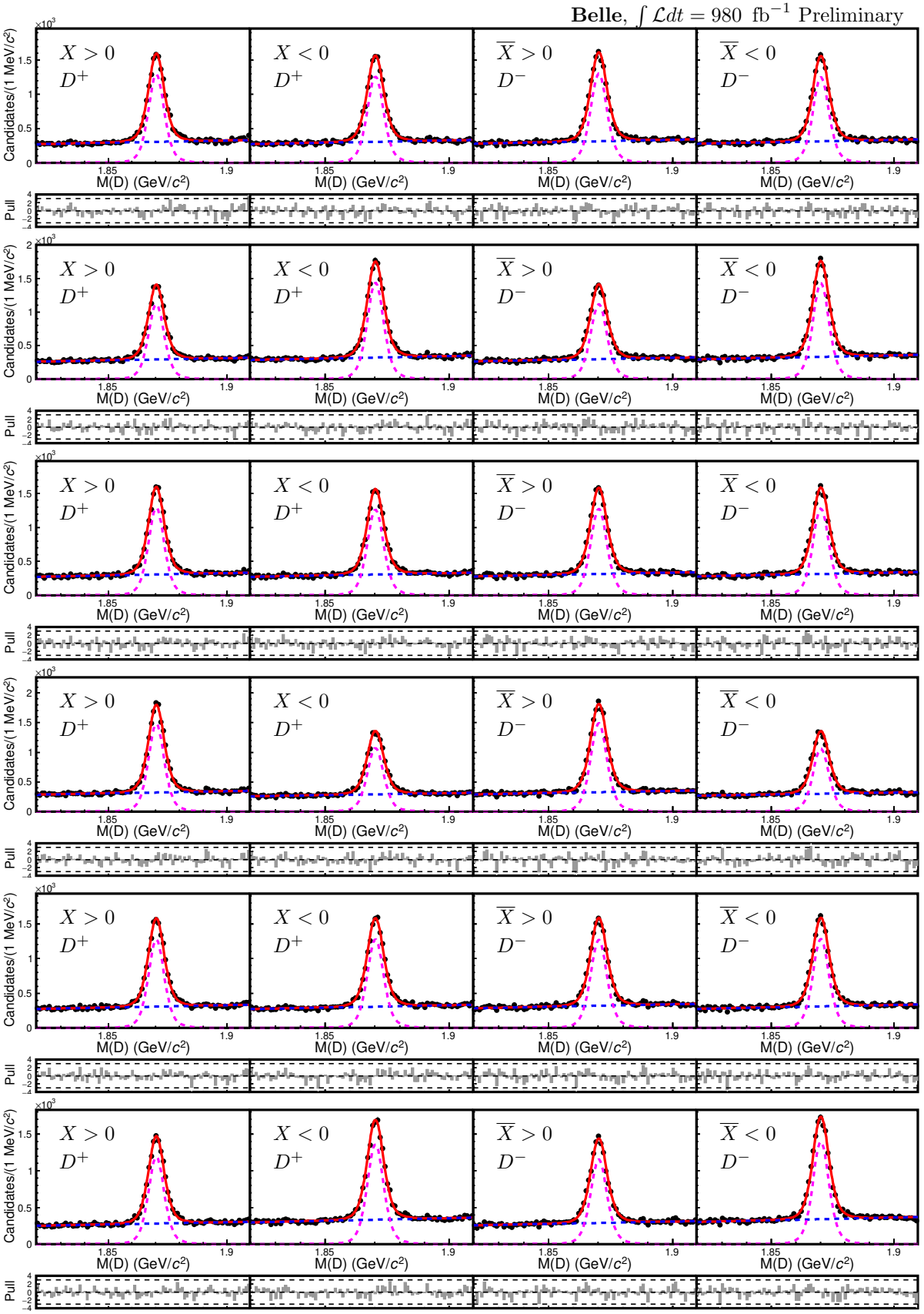

Figure 4: Fitted distributions for Belle $D^{\pm} \to K^0_S K^{\mp}\pi^{\pm}\pi^{\pm}$ data, for (top to bottom) $X = C_{\rm TP}$, $C_{\rm QP}$, $C_{\rm TP}C_{\rm QP}$, $\cos\theta_{K^0_S}\cos\theta_{K^-}$, $C_{\rm TP}\cos\theta_{K^0_S}\cos\theta_{K^-}$, and $C_{\rm QP}\cos\theta_{K^0_S}\cos\theta_{K^-}$. The red dashed curves show the fitted signal, and the blue dash-dotted curves show the fitted background. The smaller plots show the pull distributions.

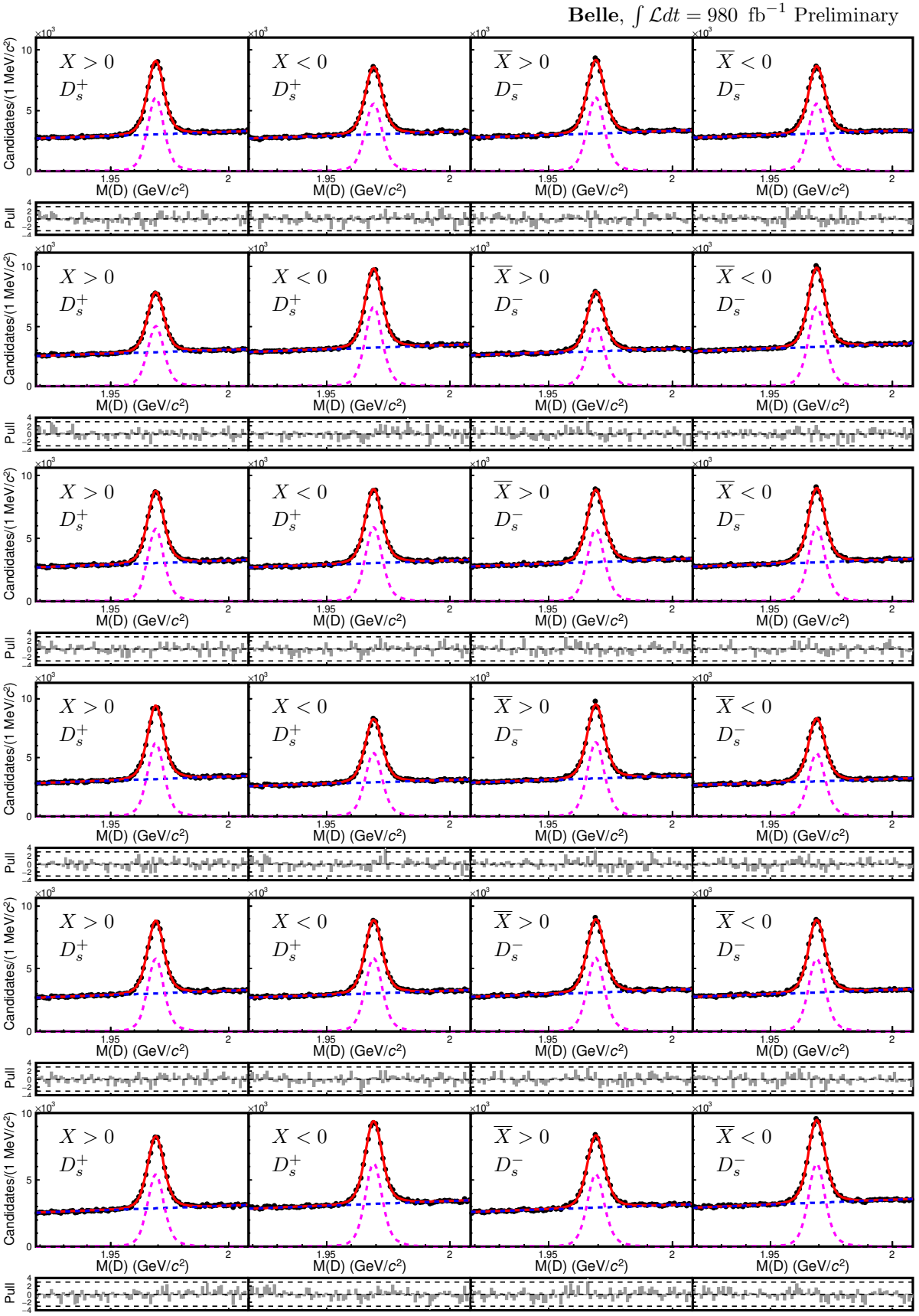

Figure 5: Fitted distributions for Belle $D_s^\pm \to K_S^0 K^\mp \pi^\pm \pi^\pm$ data, for (top to bottom) $X = C_{\rm TP}$, $C_{\rm QP}$, $C_{\rm TP}C_{\rm QP}$, $\cos\theta_{K_S^0}\cos\theta_{K^-}$, $C_{\rm TP}\cos\theta_{K_S^0}\cos\theta_{K^-}$, and $C_{\rm QP}\cos\theta_{K_S^0}\cos\theta_{K^-}$. The red dashed curves show the fitted signal, and the blue dash-dotted curves show the fitted background. The smaller plots show the pull distributions.

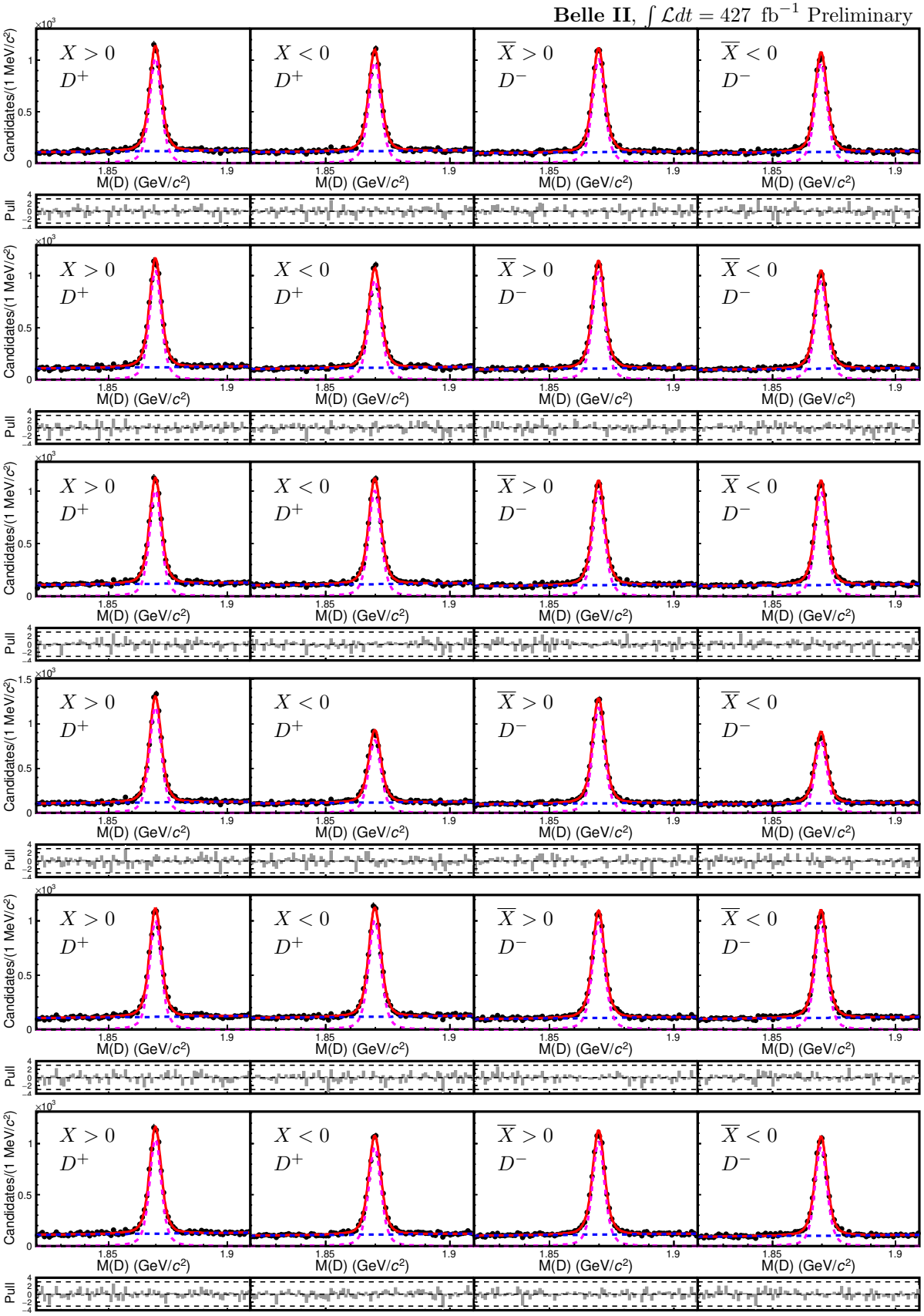

Figure 6: Fitted distributions for Belle II $D^\pm \to K^0_S K^\mp \pi^\pm \pi^\pm$ data, for (top to bottom) $X = C_{\rm TP}$, $C_{\rm QP}$, $C_{\rm TP}C_{\rm QP}$, $\cos\theta_{K^0_S}\cos\theta_{K^-}$, $C_{\rm TP}\cos\theta_{K^0_S}\cos\theta_{K^-}$, and $C_{\rm QP}\cos\theta_{K^0_S}\cos\theta_{K^-}$. The red dashed curves show the fitted signal, and the blue dash-dotted curves show the fitted background. The smaller plots show the pull distributions.

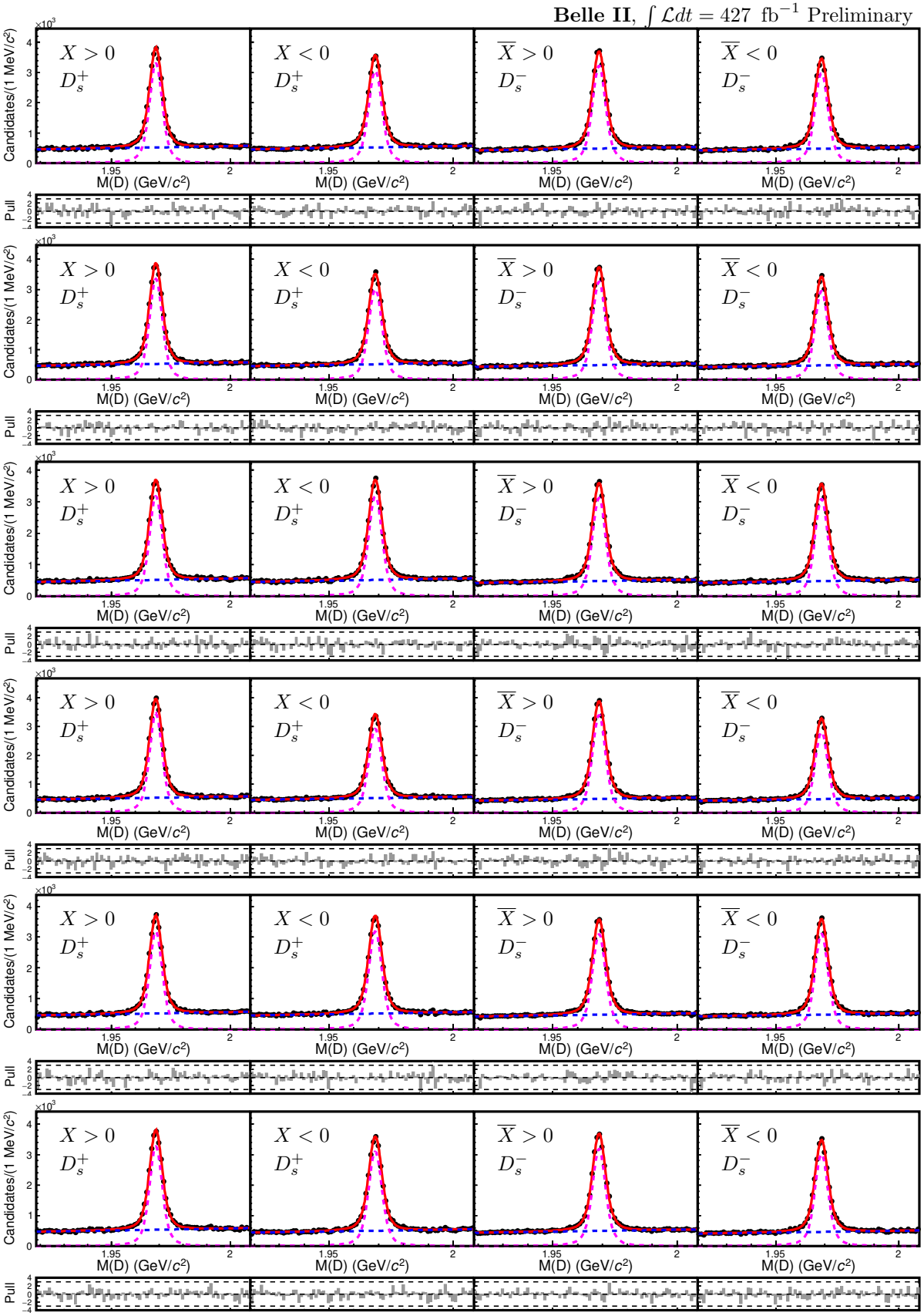

Figure 7: Fitted distributions for Belle II $D_s^\pm \to K_S^0 K^\mp \pi^\pm \pi^\pm$ data, for (top to bottom) $X = C_{\rm TP}$, $C_{\rm QP}$, $C_{\rm TP}C_{\rm QP}$, $\cos\theta_{K_S^0}\cos\theta_{K^-}$, $C_{\rm TP}\cos\theta_{K_S^0}\cos\theta_{K^-}$, and $C_{\rm QP}\cos\theta_{K_S^0}\cos\theta_{K^-}$. The red dashed curves show the fitted signal, and the blue dash-dotted curves show the fitted background. The smaller plots show the pull distributions.